# SPECIAL PROJECT PROGRESS REPORT

Progress Reports should be 2 to 10 pages in length, depending on importance of the project. All the following mandatory information needs to be provided.

**Reporting year**

2018

**Project Title:**

Deep Vertical Propagation of Internal Gravity Waves

**Computer Project Account:**

SPDESCAN

**Principal Investigator(s):**

Dr. Andreas Dörnbrack
Dr. Sonja Gisinger
Dr. Benedikt Ehard
Dr. Klaus-Peter Hoinka

**Affiliation:**

DLR Oberpfaffenhofen
Institut für Physik der Atmosphäre
Münchener Str. 20

**D – 82230 WESSLING**

Germany

**Name of ECMWF scientist(s) collaborating to the project**
(if applicable)

Dr. Nils Wedi
Dr. Christian Kühnlein
Dr. Piotr K Smolarkiewicz

**Start date of the project:**

1 January 2018

**Expected end date:**

2020

## Computer resources allocated/used for the current year and the previous one

(if applicable)
Please answer for all project resources

| | | Previous year | | Current year | |
|---|---|---|---|---|---|
| | | Allocated | Used | Allocated | Used |
| **High Performance Computing Facility** | (units) | 100000 | 100000 | 500000 | 110000 |
| **Data storage capacity** | (Gbytes) | 80 | 80 | 80 | 80 |

## Summary of project objectives

(10 lines max)

During the recent years, ground-based and airborne Rayleigh lidar measurements of temperature perturbations in the middle atmosphere show gravity wave activity covering a large spectrum of frequencies and vertical and horizontal wavelengths. An understanding of the different wave modes in the middle atmosphere is still lacking. Especially, the link of the observed gravity wave activity to possible sources in the troposphere as well as in the stratosphere is difficult to establish as 3D data of wind and temperature in high spatial and temporal resolution are missing. Therefore, the integrated forecast system (IFS) of the ECMWF will serve to fill this gap by providing these data globally. One example of the feasibility to simulate stratospheric gravity waves is documented in Dörnbrack et al. (2017). Idealized numerical simulations will complement the combined analysis of data and IFS output. Thus, the project is based on three ingredients.

## Summary of problems encountered

no problems encountered

## Summary of results of the current year

**(1) Comparison of middle atmosphere lidar data with IFS** (Ehard et al., Q. J. Roy. Met. Soc., 2018)

In addition to the analyses of the Stratospheric Task Force (Politchuk et al) we also compared the output of the IFS with not assimilated middle atmosphere temperature measurements in northern Scandinavia. The results are documented in the paper by Ehard et al. (2018): Middle atmospheric lidar temperature observations conducted above Sodankylä, Finland (67.4°N, 26.6°E), during December 2015 are compared to two estimates of the atmospheric state computed by the integrated forecast system (IFS) of the European Centre for Medium-Range Weather Forecasts (ECMWF). The first set corresponds to an hourly sampling of the middle atmosphere by the high-resolution analyses and very short-range forecasts produced by the operational IFS cycle 41r1 at a horizontal resolution of 16 km. The second set is retrieved from the upgraded IFS cycle 41r2 (horizontal resolution at 9 km) which was running in parallel with cycle 41r1 during the validation before it became operational. A remarkable agreement between both IFS data sets and the lidar temperature observations above Sodankylä is found below 45 km altitude. Above 45 km altitude, within the sponge layer of the IFS, both IFS data sets depict lower temperatures than the observations, with the 9 km runs showing the coldest temperatures. Various sensitivity experiments conducted with the IFS are analyzed and compared to the lidar observations to investigate the impact of the different changes implemented in the IFS cycle 41r2. It is found that both the scientific changes and the horizontal resolution upgrade contribute to the colder mesosphere above Sodankylä. The data assimilation seems to amplify this effect even further.

**(2) Meteorological Conditions during DEEPWAVE** (Gisinger et al., Mon. Wea. Rev., 2017)

In a comprehensive overview, different meteorological analyses from the IFS and other global NWP models are used to describe the atmospheric conditions during the DEEPWAVE campaign in austral winter 2014. Different datasets and diagnostics are combined to characterize the background atmosphere from the troposphere to the upper mesosphere. We report on how weather regimes and the atmospheric state compare to climatological conditions and also explore how they relate to the airborne and ground-based gravity wave

observations. Key results of this study are the dominance of tropospheric blocking situations and low-level south-westerly flows over New Zealand during June, July, and August 2014.

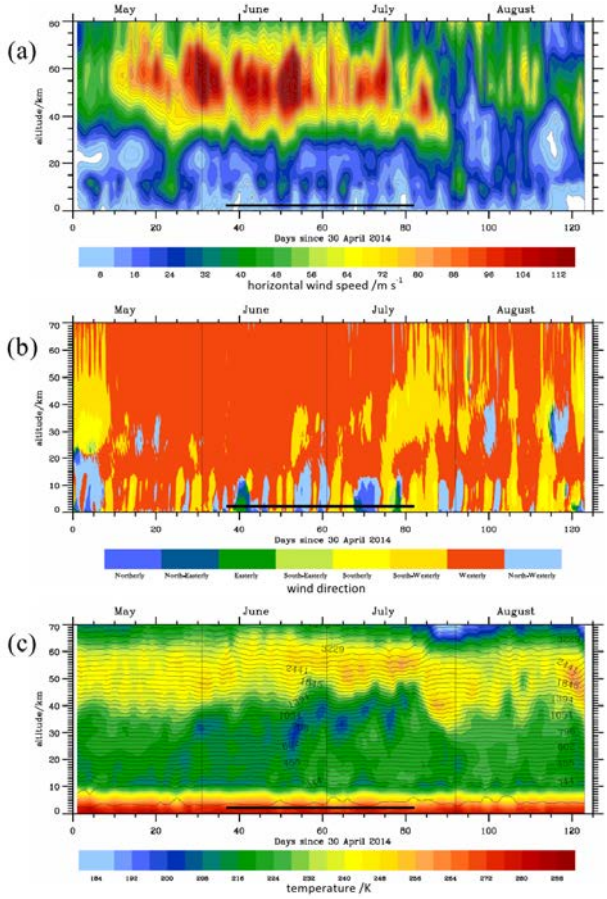


**Figure 1**: Vertical profiles of ECMWF $T_L1279/L137$ operational analyses averaged over the area between 40°S to 50°S and 165°E to 180°E. (a) horizontal wind speed (m $s^{-1}$, color shaded), (b) wind direction (binned in 45° segments centered around the given wind directions), and (c) temperature (K, color shaded) and potential temperature (K, solid lines). The black solid horizontal lines in each panel mark the DEEPWAVE aircraft deployment period.

A varying tropopause inversion layer was found to be connected to varying vertical energy fluxes and is, therefore, an important feature with respect to wave reflection. The subtropical jet was frequently diverted south from its climatological position at 30°S and was most often involved in strong forcing events of mountain waves at the Southern Alps. The polar front jet was typically responsible for moderate and weak tropospheric forcing of mountain waves. The stratospheric planetary wave activity amplified in July leading to a displacement of the Antarctic polar vortex. This reduced the stratospheric wind minimum by about 10 m $s^{-1}$ above New Zealand making breaking of large amplitude gravity waves more likely. Satellite observations in the upper stratosphere revealed that orographic gravity wave variances for 2014 were largest in May, June and July, i.e. the period of the DEEPWAVE field phase.

## (3) Case Studies of deep vertical gravity wave propagation

We have submitted and published several case studies on deep vertically propagating gravity waves, see the list of references and the status of the individual papers. Here, we report on the paper by Rapp et al. on "An intercomparison of stratospheric gravity wave potential energy densities from METOP GPS radio occultation measurements and ECMWF model data".

Temperature profiles based on radio occultation (RO) measurements with the operational European METOP satellites are used to derive monthly mean global distributions of stratospheric (20–40 km) gravity wave (GW) potential energy densities ($E_P$) for the period July 2014–December 2016. In order to test whether the sampling and data quality of this data set is sufficient for scientific analysis, we investigate to what degree the METOP observations agree quantitatively with ECMWF operational analysis (IFS data) and reanalysis (ERA-Interim) data. A systematic comparison between corresponding monthly mean temperature fields determined for a latitude–longitude–altitude grid of 5° by 10° by 1 km is carried out. This yields very

low systematic differences between RO and model data below 30 km (i.e., median temperature differences is between −0.2 and +0.3 K), which increases with height to yield median differences of +1.0 K at 34 km and +2.2 K at 40 km. Comparing $E_P$ values for three selected locations at which also ground-based lidar measurements are available yields excellent agreement between RO and IFS data below 35 km. ERA-Interim underestimates $E_P$ under conditions of strong local mountain wave forcing over northern Scandinavia which is apparently not resolved by the model. Above 35 km, RO values are consistently much larger than model values, which is likely caused by the model sponge layer, which damps small-scale fluctuations above ~ 32 km altitude. Another reason is the well-known significant increase of noise in RO measurements above 35 km.

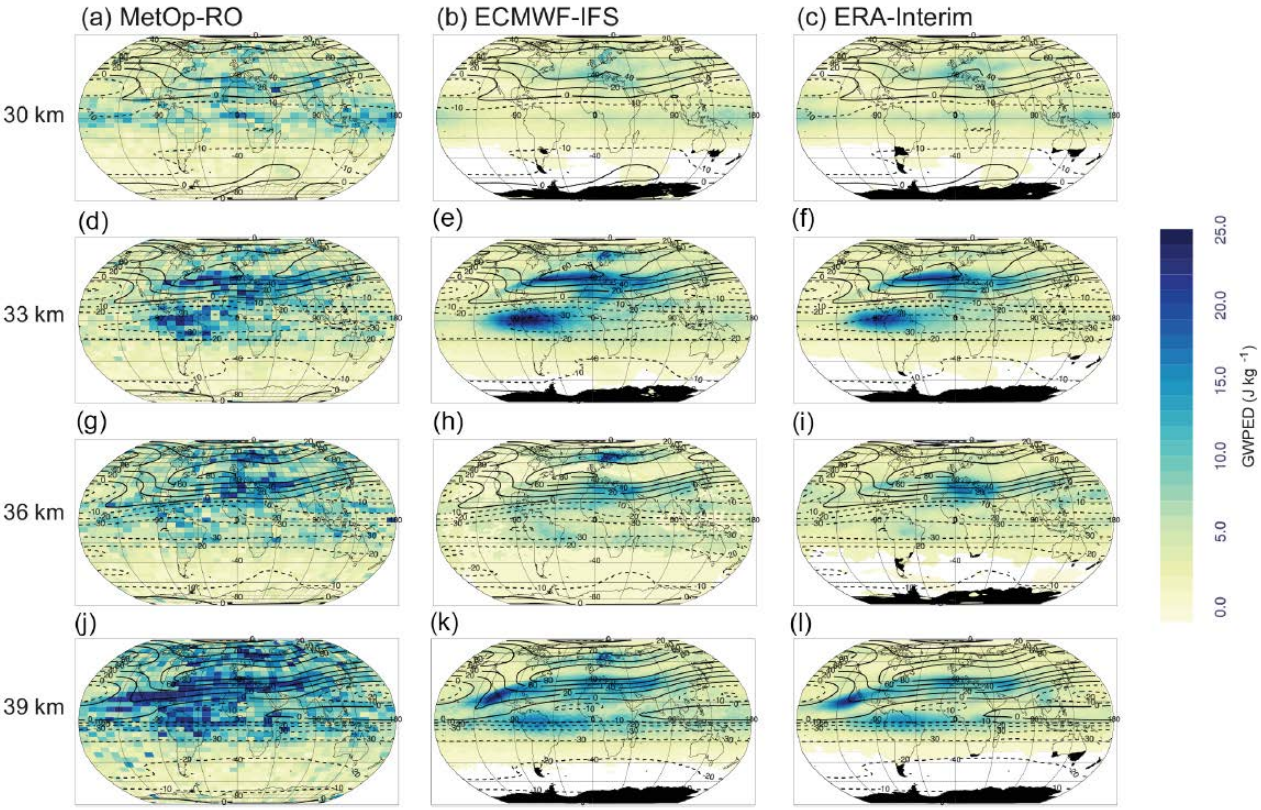


Figure 2: Monthly mean latitude–longitude cross sections of gravity wave potential energy density at selected altitudes of 30, 33, 36, and 39 km (a–l) for December 2015. (a, d, g, j) METOP RO-dry data, (b, e, h, k) IFS data, and (c, f, i, l) ERA-Interim data. In all panels, black contour lines show zonal wind values from ERA-Interim.

The comparison between RO and lidar data reveals very good qualitative agreement in terms of the seasonal variation of $E_P$, but RO values are consistently smaller than lidar values by about a factor of 2. This discrepancy is likely caused by the very different sampling characteristics of RO and lidar observations. Direct comparison of the global data set of RO and model $E_P$ fields shows large correlation coefficients (0.4–1.0) with a general degradation with increasing altitude. Concerning absolute differences between observed and modeled $E_P$ values, the median difference is relatively small at all altitudes (but increasing with altitude) with an exception between 20 and 25 km, where the median difference between RO and model data is increased and the corresponding variability is also found to be very large. The reason for this is identified as an artifact of the $E_P$ algorithm: this erroneously interprets the pronounced climatological feature of the tropical tropopause inversion layer (TTIL) as GW activity, hence yielding very large $E_P$ values in this area and also large differences between model and observations. This is because the RO data show a more pronounced TTIL than IFS and ERA-Interim. We suggest a correction for this effect based on an estimate of this artificial $E_P$ using monthly mean zonal mean temperature profiles. This correction may be recommended for application to data sets that can only be analyzed using a vertical background determination method such as the METOP data with relatively scarce sampling statistics. However, if the sampling statistics allows, our analysis also shows that in general a horizontal background determination is advantageous in that it better avoids contributions to $E_P$ that are not caused by gravity waves.

**(4) Inversion of potential vorticity** (Egger, Hoinka, and Spengler, J. Atmos. Sci. 2017)

Inversion of potential vorticity density $P_\eta^* = (\omega_a \nabla\eta)/(\partial\eta/\partial z)$ with absolute vorticity $\omega_a$ and function $\eta$ is explored in $\eta$ coordinates. This density is shown to be the component of absolute vorticity associated with the vertical vector of the covariant basis of $\eta$ coordinates. This implies that inversion of $P_\eta^*$ in $\eta$ coordinates is a two-dimensional problem in hydrostatic flow. Examples of inversions are presented for $\eta = \theta$ ($\theta$ is potential temperature) and $\eta = p$ ($p$ is pressure) with satisfactory results for domains covering the North Pole. The role of the boundary conditions is investigated and piecewise inversions are performed as well. The results shed new light on the interpretation of potential vorticity inversions.

**(5) The vertical component of the geostrophic wind** (Egger and Hoinka, Q. J. Roy. Meteorol. Soc., 2018)

Motion in planetary geostrophic equations (PGE) is represented by the three dimensional geostrophic wind ($u_g$, $v_g$, $w_g$) where $u_g$ and $v_g$ are the standard horizontal components while the vertical component $w_g$ can be derived, for example, from the Richardson equation. However, this vertical component appears not to have been evaluated as yet on the basis of data nor compared to the actual vertical component w. Part of this missing information is provided here by an evaluation of $w_g$ from observations and by analyzing the role of $w_g$ in linear versions of PGE. The time-mean fields $\widehat{w}_g$ in the northern hemisphere as well as the standard deviations $\sigma_{wg}$ are compared to the corresponding fields of w. It is found that $\widehat{w}_g$ comes reasonably close to $\widehat{w}$ in the troposphere but deviates widely in the stratosphere while $\sigma_{wg}$ is smaller than $\sigma_w$ in the troposphere but not in the stratosphere. Linear wave motion is discussed and the linear steady-state response to the forcing by heat sources and mountains is explored to explain these results.

## List of publications/reports from the project with complete references


1. Woiwode, W., A. Dörnbrack, M. Bramberger, F. Friedl-Vallon, F. Haenel, M. Höpfner, S. Johansson, E. Kretschmer, I. Krisch, T. Latzko, H. Oelhaf, J. Orphal, P. Preusse, B.-M. Sinnhuber, and J. Ungermann, 2018: Mesoscale fine structure of a tropopause fold over mountains, submitted to *Atmos. Chem. Phys. Discuss*, 22 June 2018; https://doi.org/10.5194/acp-2018-625, in review, 2018.

2. Fritts, D. C., S. B. Vosper, B. P. Williams, K. Bossert, M. J. Taylor, P.-D. Pautet, S. D. Eckermann, C. G. Kruse, R. B. Smith, A. Dörnbrack, M. Rapp, T. Mixa, I. M. Reid, and D. J. Murphy, 2018: Large-Amplitude Mountain Waves Accompanying Weak Cross-Mountain Flow During DEEPWAVE Research Flight RF22 on 13 July 2014. *J. Geophys. Res*., submitted 28 Dec 2017, 2nd revision resubmitted 30 May 2018; accepted June 2018.

3. Chu, X., J. Zhao, X. Lu, V. L. Harvey, R. M Jones, C. Chen, W. Fong, Z. Yu, B. R. Roberts, and A. Dörnbrack, 2018: Lidar observations of stratospheric gravity waves from 2011 to 2015 at McMurdo (77.84° S, 166.69° E), Antarctica: Part II. Potential energy densities, lognormal distributions, and seasonal variations. *J. Geophys. Res*., submitted 1. July 2017, minor revision 21 September 2017; resubmitted March 2018; accepted 20 June 2018

4. Ehard, B., S. Malardel, A. Dörnbrack, B. Kaifler, N. Kaifler, and N. Wedi, 2018: Comparing ECMWF high resolution analyses to lidar temperature measurements in the middle atmosphere. submitted to *Q. J. R. Met. Soc.* 16.4.2017; minor revions, 20 September 2017, resubmitted 30 October 2017; accepted 8 November 2017

5. Rapp, M., Dörnbrack, A., and Kaifler, B., 2018: An intercomparison of stratospheric gravity wave potential energy densities from METOP GPS radio occultation measurements and ECMWF model data, *Atmos. Meas. Tech*., **11**, 1031-1048, https://doi.org/10.5194/amt-11-1031-2018.

6. Portele, T. C., A. Dörnbrack, J.S. Wagner, S. Gisinger, B. Ehard, P. Pautet, and M. Rapp, 2018: Mountain-Wave Propagation under Transient Tropospheric Forcing: A DEEPWAVE Case Study. *Mon. Wea. Rev.*, **146**, 1861–1888, https://doi.org/10.1175/MWR-D-17-0080.1

7. Bramberger, M., A. Dörnbrack, K. Bossert, B. Ehard, D. C. Fritts, B. Kaifler, C. Mallaun, A. Orr, P.-D. Pautet, M. Rapp, M. J. Taylor, S. Vosper, B. Williams, and B. Witschas, 2017: Does strong tropospheric forcing cause large-amplitude mesospheric gravity waves? - A DEEPWAVE Case Study. *Journal of Geophysical Research: Atmospheres*, **122**, *11,422–11,443.* https://doi.org/10.1002/2017JD027371

8. Gisinger, S., A. Dörnbrack, V. Matthias, J. D. Doyle, S. D. Eckermann, B. Ehard, L. Hoffmann, B. Kaifler, C. G. Kruse, and M. Rapp, 2017: Atmospheric Conditions during the Deep Propagating Gravity Wave Experiment (DEEPWAVE), *Mon. Wea. Rev*., **145**, 4249-4275: https://doi.org/10.1175/MWR-D-16-0435.1

9. Egger, J., K. Hoinka, and T. Spengler, 2017: Inversion of Potential Vorticity Density. *J. Atmos. Sci.*, **74**, 801–807, https://doi.org/10.1175/JAS-D-16-0133.1

10. Egger, J. and K. Hoinka, 2018: The vertical component of the geostrophic wind. *Q. J. R. Meteorol. Soc.* **143**: 1704–1713.

## Summary of plans for the continuation of the project

(10 lines max)

We continue like planned and outlined in the proposal.